MÁSTERES de la UAM

Facultad de Ciencias /12-13

Máster en Física de la Materia Condensada y Nanotecnología

Aggregation effects in iron oxide nanoparticles for Hyperthermia

Jesús García Ovejero

UNIVERSIDAD AUTONOMA DE MADRID

Campus Internacional
excelencia UAM CSIC+

UAM EDICIONES

INDEX

1. INTRODUCTION

1.1 NANOPARTICLES IN MEDICINE

Some years ago, Nanoscience was a revolutionary and multidisciplinary framework for scientist who tried to understand the laws that control the nature at nanometric scale. At the same time, industry has been interested in extracting possible applications of the new properties that matters presents when its dimensions are reduced.

Nowadays many of these issues have begun to become reality. It is easy observed around us technological advantages that would not be possible without the development of this field. Some of the most promising are the new medical facilities based on nano-objects. This master work intends to be a contribution to the field.

The main goal is to study the magnetic properties of iron oxide nanoparticles their use in a revolutionary cancer therapy approach called Hyperthermia. The Hyperthermia takes advantage of the heat generated by magnetic nanoparticles (MNP) submitted to an alternating magnetic field to warm up a tumoral tissue. The rising of the temperature can induce the death of tumoral cells. (Jordan, Endocytosis of destran and silan-coated nanoparticles and the effect of intracillular hyperthermia on human mammary carcinoma cells in vitro, 1999)

The first attempt was performed by Gilchrist in 1957 (Gilchrist, 1957) when magnetic microparticles were used to attack lymph nodes. However the development of new physicochemical synthesis to produce MNP with better features for this proposal has improved the efficiency of the technique and reduced the side effects. One of the first *in vivo* trials with MNP was carried out in mice by Chang (Chang, 1993) and Jordan (Jordan, Inductive heating of ferrimagnetic particles and magnetic fluids: Physical evaluation of thier potential for hyperthermia., 1993) with hopeful results. The most recent studies, (Lee, 2011) have demonstrated not just the capacity of stopping the growth of the tumor, but moreover the possibility of reducing it, improving the patient quality of life.

The main advantage of this technique is the possibility of localizing the effects of the treatment in the ill tissue driving the nanoparticles with external magnetic fields (Mejías, 2011) or by direct injection. This is not possible in the rest of actual cancer treatments – radio- and chemotherapy – which present global response and harmful side effects. Furthermore, the

use of nanoparticles allows the combination of Hyperthermia with other innovations as drug delivery, producing a synergic effect of both techniques. (Brazel, 1996) (Chilkoti, 2002).

In spite of all these landmarks and advantages, many fundamental aspects of the ferrofluids require deeper studies. One of them is the study of the aggregation effects on the magnetic properties of the nanoparticles during the internalization into the cells.

When the nanoparticles are phagocyted by the cells they remain encapsulated in vesicles (see fig 1). This encapsulation changes the distance between the particles and their magnetic interactions. Consequently, *in-vitro* experiments show that the heat generated by the MNP is lower inside the cells (J.p. Fortin, 2008).
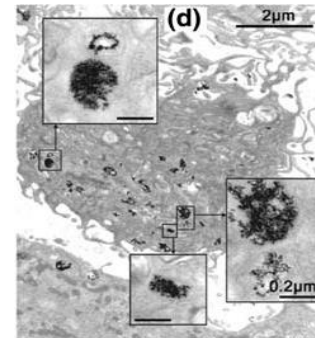

Fig 1. Internalization of maghemite nanoparticles in PC3 tumor cells. (J.p. Fortin, 2008)

This work intends to study the influence of iron oxide nanoparticle aggregation state in their magneto-caloric properties. That would help to understand the magneto-thermal behavior inside cells.

1.2 IRON OXIDE NANOPARTICLES

There are many magnetic materials that contest for being the best candidate for this novel technique, e. g., iron oxides (Fe_3O_4 and γ-Fe2O3), cobalt ferrite, copper-nickel alloys, etc. Some of them offer high anisotropy and magnetization of saturation, features very suitable for the heat generation.

However most of these materials present a big handicap for biomedical applications, their toxicity. Usually the best candidates a priori for their magnetic properties are not appropriate for the human trials. The most promising mediators for Hyperthermia are the iron oxide nanoparticles. Although they do not present so high heating rate and are necessaries high concentrations to obtain appreciable effects, their biocompatibility and their facility to escape from the reticuloendothelial system means an enormous advantage respect to their competitors (Mahmoudi M., 2009) (A. Villanueva, 2009).

The second crucial condition for the scalability to human treatment is the colloidal stability of the nanoparticles. The dangers of the coagulation are evident when we think in the injection of the nanoparticles in the circulatory system. However, the presence of massive objects in the veins is given to produce obstructions in the smallest capillaries, and thrombi are

consequences not assumable for any medical treatment. The MNP size provides also the option to anchor a wide variety of coatings that ensure their stability at physiological pH.

1.3 HEATING DISSIPATION PROCESS IN MAGNETIC NANOPARTICLES

As was mentioned at the beginning, at nanoscale the matter presents very different properties, and this also occurs in the case of MNP. When we decrease the size of a magnetic system, we reduce the number of magnetic domains until the point where the monodomain structure is the most energetically favorable arrangement.

At this point, the whole nanoparticle behaves like a single magnetic moment and the coercitivity is maxima. But if we continue decreasing the size, the thermal fluctuations become more and more important, and the moment of the nanoparticle starts to flip between two positions energetically equivalents, this is known as *superparamagnetic behavior*. Because that, it does not presents any remanence and the hysteresis loops appears closed under quasi-static field conditions (Getzlaff, 2008). If the hysteresis loop is closed the system does not dissipate energy.

Nevertheless, if the applied field is faster than the thermal fluctuation, the magnetic moment of MNP suffers a lag to follow the external magnetic field and starts to dissipate energy again. Hence, it is possible to extract heat from superparamagnetic nanoparticles applying fields speed enough.

Based on Stoner-Wohlfarth model, Rosensweig (Rosensweig, 2002) developed the first serious theoretical approximation to the problem. He considered the energy dissipated by a magnetic system introducing an out-of-phase component to the magnetic susceptibility χ''.

$$\Delta U = 2\,\mu_0\,H_0^2\chi''\int_0^{\frac{2\pi}{\omega}} \sin^2 \omega t \, dt \qquad (1)$$

Where μ_0 is the vacuum magnetic permeability and H_0 is the applied field. Solving the integral and multiplying by the frequency of the system (f) it is possible to obtain the heat dissipated by the ferrofluid.

$$\text{P} = f\,\Delta U = \mu_0\pi\,\chi'' f H_0^2 \qquad (2)$$

In the imaginary component are contained all the dissipation mechanism of the ferrofluid, which can be related with the relaxation time of the system (τ) and its modulus (χ$_0$)

$$\chi'' = \frac{\omega\tau}{1+(\omega\tau)^2}\,\chi_0 \qquad (3)$$

Relaxation time presents two possible origins:

- **Neél relaxation τ_N**, when the nanoparticle moment rotates respect to the crystalline structure crossing hard axes.

$$\tau_N = \frac{\sqrt{\pi}}{2}\tau_0 \frac{\exp \Gamma}{\sqrt{\Gamma}} \quad (4)$$

The amount of heat dissipated will depend on the magnetic hardness of the material. This property is quantified by the factor $\Gamma = \kappa V/K_B T$, where κ is the anisotropy constant and V is the volume of the nanoparticle (Brown, 1963). This relaxation is present when the nanoparticles are small due to its exponential growth with the size of the MNP.

- **Brownian relaxation τ_B**, when the whole nanoparticle moves in concordance with the magnetic moment and keep it fixed respect to MNP easy axis.

$$\tau_B = \frac{3\eta V_H}{K_B T} \quad (5)$$

The capacity of the MNP to rotate depends on its hydrodynamic volume V_H, the viscosity of the media η and the temperature (Frenkel, 1855). The bigger the nanoparticle the more important is the Brownian relaxation because the interactions with the media are stronger.

The mechanism responsible of energy dissipation is always the faster, in other words, the one with shorter relaxation time. So both relaxation times can be gathered in the following expression.

$$\frac{1}{\tau} = \frac{1}{\tau_N} + \frac{1}{\tau_B} \quad (6)$$

To determinate the contribution of each mechanism, many parameters must be taken into account, e. g., the size, the anisotropy constant of the material, the composition of the coating, etc. This is the base of the first part of the work. To carry out this study it will be necessary to synthetize nanoparticles with very narrow size distribution and low dispersity in aggregate sizes in order to have an uniform behavior in our systems (Hergt, 2008) (Mehdaoui, 2011).

Consequently, this has supposed a priority during the preparation of the nanoparticles and has been determinant to choose the synthesis methods.

2. SYNTHESIS AND COATING

The first step of the work is the synthesis of the nanoparticles. For this propose we have used three methods that provide uniform nanoparticles of different sizes, the co-precipitation of Fe(II) and Fe(III), the decomposition in organic media and precipitation of Fe(II).

There exist many other methods to obtain stable ferrofluids (Durdureanu-Angheluta, Materials Science and Technology: Tailored and Functionalized Magnetite Particles for Biomedical and Industrial Applications, 2012) with different features as size, crystallinity, shape, etc. But the three chosen methods produce MNP with a distribution of sizes narrow enough for this study.

To obtain these uniform nanoparticles, in the three syntheses the nucleation and growth process must be tailored to obtain a certain number of nuclei with a controlled growth time.

2.1 Co-precipitation

The co-precipitation is based in the method developed by Massart in 1981 (Massart, 1981). It has proved to be a very successful procedure because its simplicity and low cost. In fact this is the method applied in the commercial synthesis of ferrofluids. (I. Martinez-Mera, 2007)

The description of Massart involves the mix of two iron salts $FeCl_3 \cdot 6H_2O$ and $FeCl_2 \cdot 4H_2O$ both prepared in HCl. When both salts are mixed, a base (NH_4OH) is added rapidly with vigorous stirring producing the fast formation of the little magnetite beads.

After some magnetic separations and cleanings we obtain a stable solution of magnetite. The origin of this stability resides in the presence of OH^- groups at the surface of the nanoparticle. That is because the oxygen of the nanoparticle tends to bond these groups around and create a charged surface that repels each other (Durdureanu-Angheluta, 2008).

The speed of the reaction does not allow the well arrangement of the surface atoms. Therefore, the product is a ferrofluid with low crystallinity. An acid treatment and a recrystallization process will produce a phase transition from magnetite to maghemite, and a correction of the surface defects respectively.

The final product is a colloidal suspension of maghemite nanoparticles in water, stable at pH 3. They will need to be coated to be also stable at pH 7.

2.2 THERMAL DECOMPOSITION IN ORGANIC MEDIA

Despite the simplicity of the co-precipitation synthesis, other routes are required to produce bigger nanoparticles. The second route used is decomposition in organic media.

This method begins with an oleate of iron that presents a metallic center of iron (III) attached to a three organic chains. The key point of this oleate is that the bonds with the organic chains can be sequentially broken rising the temperature (Pachoudhury, 2011) and the aggregation of the metallic centers can be tuned adjusting the temperature and the time process of the process.

Actually, the synthesis of iron oxide nanoparticles is possible thanks to the difference in the temperatures of the nucleation and growth (Park, 2004). The nucleation occurs at 200-240 ºC when the two first oleate's ligands are detached from the precursor. But the growth of the seeds doesn't begin until the third ligand is detached too. And due to the strongest bond of this third ligand, this process starts at 250 ºC and works effectively around 300 ºC.

The process has been well proved by thermo-gravimetric analysis (technique explained in the following chapter) performed at different steps of the process. The separation of nucleation and growth processes allows the tune of the particles size in a uniform way, obtaining particles between 15 and 20 nm with a narrow distribution of sizes.
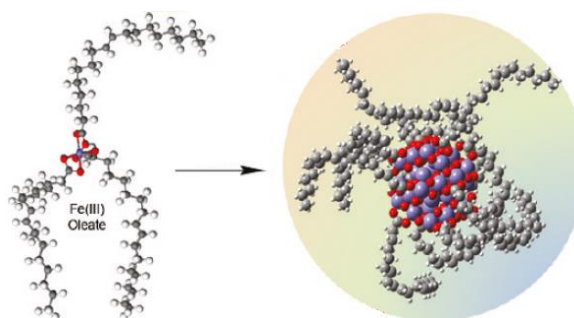

Fig 2. Scheme of the iron oleate and iron oxide nanoparticle formed by thermal decomposition in organic media

This revolutionary route was first reported by A. P. Alivisatos in 1999 (Alivisatos, 1999), and it has been developed with different solvents, times and environmental conditions to obtain MNP with a wide variety of shapes and sizes (Salas, 2012). The main drawback is that it requires a solvent with a high boiling point so that the nucleation and growth temperatures could be reached in the suspension. Hence, it is necessary to use a surfactant, which afterwards, must be exchange by other molecule to make the particles stable in water.

The process followed consist in a controlled heating of an oleate of Iron (III) solved in octadecene with two ramps of temperature that control the time of nucleation and growth respectively. The final product consists on MNP dispersed in hexane and coated of oleic acid chains. The exchange of coating will be explained in point 2.4.

2.3   Precipitation of iron (II)

The last method of synthesis was developed by Sugimoto and Matijević in 1979 (Matijevic, 1979) and has become a good chance to prepare large magnetite nanoparticles. In fact, it was initially described to form magnetic microparticles. However controlling carefully different parameters is possible to obtain nanoparticles between 20 and 100 nm.

It consists in a sol-gel method where magnetite nanoparticles are formed from the mix of a KOH and $FeSO_4$ solution in the presence of a mild oxidant (KNO_3). The mix is aged at 90ºC during 24 hours in anoxic conditions. After this time the desired size have been reached and it only rest to remove the rest of the products, Fe^{2+} ions and $Fe(OH)_2$.

Fig 3. Size and dispersion obtained from the precipitation method in function of reactants concentration (Matijevic, 1979)

The size and the dispersity of the nanoparticles depend on the excess of reactants in the sol-gel ($[Fe^{2+}]_{excess}$=[FeSO4]-$\frac{[KOH]}{2}$ or $[OH]_{excess}$=[KOH]-2[FeSO4]) as show the fig 3. Small excess of Fe^{2+} leads to the mean size of 25 nm and the size distribution around 20%.

2.4   Coating

The general tendency of the atoms is to aggregate each other and form a bulk state reducing as much as possible the surface energy. Hence, if we want to create systems composed by stable isolated crystals, we must introduce repulsive forces between them and avoid the aggregation process.

This force can be introduced in two ways. Using steric barriers, where a coating is added as a physical barrier between the parts that must be isolated; or by Coulombian forces, adding to the MNP surface charges that introduces repulsions between them.

The first way is usually performed with polymers attached at the nanoparticle surface, e. g., polyethylene glycol. While the second, is done by the bonding of some acid or basic groups to the nanoparticle surface.

Bare MNP, as many other materials, present in their surface some hydroxyl groups that, depending on the media where they had been dispersed, can trap positive or negative charge.
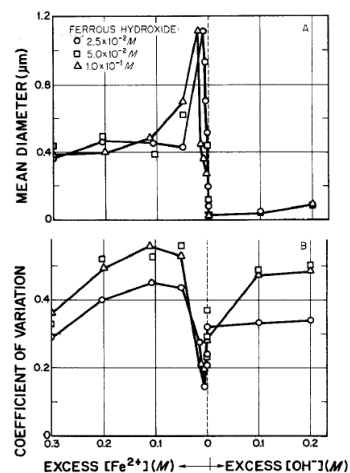
This charge is attached at the surface covalently but in order to compensate it, the media places ions with opposite charges around, creating a second diffused layer. The spread of this second layer depends on the temperature and ions in the media. This is known as the *double layer model* (Hunter, 1993).

Double layer introduces a repulsion that confers certain stability to the colloids before the coating, but it could be not enough in the case of large magnetic particles at certain pH. To obtain a thermodynamically stable colloid at physiological pH, our MNP need some extra repulsive charge. That charge has been introduced coating the nanoparticles with dimercaptosuccinic acid (DMSA), fig 4. It consists in a short chain of carbon atoms with an acid group in each end and sulfur radicals bonded in the central positions.
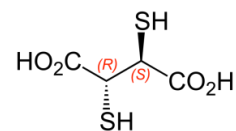

Fig 4. DMSA molecule

In the case of the nanoparticles suspended in water, the carboxylic groups react with the Fe at the surface and create a strong bond through the oxygen. The sulfurs of the chains arranged around interact each other and create a crown that covers completely the nanoparticle, fig 5.
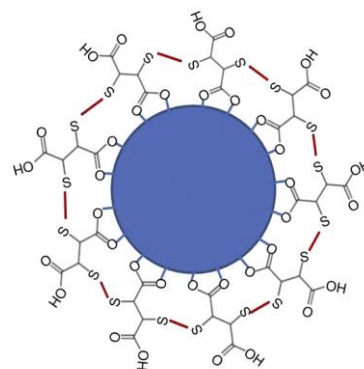
The process in organic media is quite different, in that case the MNP are already covered by chains of oleic acid and a ligand exchange process is required to replace the oleic acid by the DMSA molecule (Salas, 2012). Then the particles are stable in water at pH7.

Fig 5. DMSA crown-shape coating around an iron oxide nanoparticle. (Mejías, 2011)

The motivations for selecting the DMSA as coating are three:

- The high stability of the colloid at physiological pH.
- The possibility of attaching it to particles synthetized by the three chosen routes.
- A third very important factor is the internalization of particles with this kind of coating in tumoral cells. There are many studies that point out these particles as suitable for Hyperthermia because the cell uptake (A. Villanueva, 2009).

3. STRUCTURAL AND COLLOIDAL CHARACTERIZATION

Once that the nanoparticles have been synthetized and the colloids have been cleaned removing the unused reactants and filtering, the next step is to characterize the ferrofluid that we are going to study. In this chapter are presented the main techniques of structural and colloidal characterization.

3.1. Characterization of magnetic core

The first step is to know the characteristic of iron oxide core.

3.1.1 Mean size and size distribution

The method to measure the particle mean size, shape and size distribution is to observe a representative population of the sample and extract the statistical values for the whole sample.

For this observation two systems are commonly used. The Scanning Electron Microscopy (SEM) and the Transmission Scanning Microscopy (TEM). In our case, we study nanoparticles too small to be observed by reflection, especially if we are interested in a quantitative analysis.

Consequently, the chosen technique is the TEM. Nevertheless, it presents a big drawback because what we observe by this technique is the shadow of the particles, their projection in the plane perpendicular to the beam. Hence it requires a very careful analysis of the images.

Once that a considerable amount of particles have been registered, we will extract the mean size and the size distribution using a log normal adjustment. (Edwin L. Crow, 1988)

3.1.2 Iron oxide concentration

Many calorimetric properties of the ferrofluids are defined in function of the magnetic material concentration. That is because this parameter finds a compromise between the size and the number of particles, i. e., with the same concentration the atoms can be altogether in big clusters or separated in small seeds, but the amount of material is the same in both cases.

The technique chosen for this task is the inductively coupled plasma optical emission spectrometry (ICP-OES). It consists on a plasma that ionizes a gas evaporated from a sample with unknown concentration producing ions with different charge as a function of the atom nature, and accelerates them on a mass spectrometer. In the end, the number of counts can be related to the amount of a specific material present in the original solution.

Having into account the volume of solution introduced, it is easy to calculate the concentration of that specific element. From the concentration of iron we will be able to calculate the iron oxide concentration knowing the iron oxide phase.

3.1.3 CRYSTALLINE STRUCTURE

The chosen technique to study the crystalline structure of the MNP has been the X-ray diffraction (XRD) diagram. The positions of the peaks will reveal the crystal structure of the nanoparticles and will show the different phases present there. Unfortunately, the two basic phases present in our nanoparticles –magnetite and maghemite – have very close peaks positions in the spectra and it is not possible to resolve their maximums. But at least, we can determine that any other unwanted or non-magnetic phase is present.

Besides, the X-ray diffraction provides also very useful complementary information. The width at half maximum of a spectra peak gives the size of the crystals by using the Scherrer equation:

$$D_{XRD} = \frac{k\lambda}{B_c \cos\theta} \qquad (7)$$

Where the k is a constant factor that depends on the experimental conditions (0.9), λ is the wavelength of the X-ray used (Cu), B_c is the width of the peak (correct from the instrumental contribution), and θ is the position of the peak. If the size of the crystal and the size of our nanoparticles observed by TEM are similar, the direct conclusion is that we are dealing with monocrystalline nanoparticles.

3.2 CHARACTERIZATION OF THE COATING

Surface properties of the MNP were analyzed by different techniques to identify the coating and quantify it.

3.2.1 THERMO-GRAVIMETRIC ANALYSIS (TGA)

A minimum amount of powder, around 10 mg is required to perform a Thermo-gravimetric analysis. It consist on submitted the sample to a slope of temperature. The maximum temperature, the increasing rate and the atmosphere can be adjusted for a proper analysis. During the heating, a balance of high sensitivity measures the loss of weight. The loss of weight can show, among other features, the energy of the bonds between the coating and the magnetic core and the amount of organic material. Generally, the higher is the temperature needed to evaporate the coating the more energetic the bonds are.

3.2.2 SUPERFICIAL CHARGE AND ISOELECTRIC POINT

As we have explained in the point 2.3 the MNP presents a surface charge density responsible for the stability of the colloid. To estimate this charge, the zeta potential is used as

parameter. It represents the Coulombian potential created by the nanoparticle coating around it (Hunter, 1993), and hence the repulsion force between the particles.

The instrument used to measure the zeta potential it is called *Dynamic Light Scattering* (DLS). The DLS analysis is based on the way in which the particles scatter the light. The set up consists in a laser that impact on a cell where the colloidal suspension is placed. A photodetectors is disposed at certain angle to quantify the amount of light that is scattered by the suspension.

What this photodetectors estimate is the temporal coherence of the light emitted by the laser. The coherence will depend on the velocity of the particles in the media. Using this relation, the system is able to measure the velocity and the acceleration of the particles in the suspension. The way to relate the value of the surface charge and the velocity of the particles is measuring the acceleration of the particles when they are immersed in the field created by two electrodes placed at both sides of the cell.

The surface charge depends on the pH of the solution because it determines the structure of the ionic double layer explained in the point 2.4. The usual representation of this charge is a curve where the zeta-potential is represented at different pHs. The point where the surface charge is zero is called *isoelectric point*, and it represents the pH region at which the colloid is not stable.

3.3 Stability characterization: hydrodynamic size

The hydrodynamic size and its variation with the pH is a very relevant parameter to determine the stability of nanoparticles in a colloidal suspension. It measures how big the aggregate formed by the nanoparticles in suspension is. Therefore, it will present a great importance in our study.

This parameter is defined as the size of an equivalent sphere moving in a media with the same viscosity. To measure it the DLS is used as well. It takes advantage of the relation between *the Brownian movement* and the size of nanoparticles. This movement is bigger for the smallest particles which are more sensitive to the impacts with their environment (Hunter, 1993), and smaller for the more massive particles. From that relation the system provide an approximate value for the particles mean size (D_H) and the size distribution estimated by polydisperisty index (PDI) through their velocity of the dispersed particles.

4. MAGNETIC CHARACTERIZATION

We evaluate the MNP magnetic behavior under an alternating magnetic field by using two different experimental measurements.

4.1 CALORIMETRY MEASUREMENT SYSTEM

Calorimetry measurements allow us to determine the thermal capabilities of MNP in order to evaluate the aggregation effects. For that purpose, a homemade frequency variable system was used to generate alternating magnetic fields up to 185 kHz and 50 mT, fig 6. The coil is composed by C shape ferrite cores coiled with Litz wires and connected to a LCR circuit where the different resonant frequencies are achieved by changing capacitor value. A sinusoidal shape current is injected in the LCR circuit by a waveform signal amplified. The coils are air cooled to reduce the amount of heat introduced in the sample.

On the other hand, ferrofluid temperature is measured with a commercial optical fiber probe TS2/2 connected to a FOTEMP2-16 two-channel signal conditioner with an experimental error of ±0.2ºC. For the present study, calorimetry measurements have been performed on a 35 ml volume of ferrofluid with an iron concentration of 2.5 g/l. The sample holder is a glass flask with a vacuum shield covered by a polystyrene stopper where an upper aperture allows the introduction of a temperature probe. This system provides non-adiabatic conditions but with reduced thermal losses exchange (Teran, 2012).

After placing the sample with the temperature probe on the sample holder and waiting for thermalization with the surrounding, an alternating magnetic field is applied for a time span. Simultaneously, the software reads the temperature values every 0.5 seconds. Thus, we can follow the time variation curve of the sample temperature under given conditions of magnetic field and frequency. Afterward, we extract the initial slope from the temperature curve by fitting a straight line in the first 10 seconds where temperature follows a linear behavior due to the scarce influence of the thermal losses (appendix). The measurement is repeated three times and the considered value will be the average of the three slopes. The heat capacity of the MNP is estimated by the Specific Absorption Rate:

$$SAR = \frac{C_V}{[Fe]}\frac{dT}{dt} \qquad (8)$$

Where C_V is the volume specific heat of the dispersion, [Fe] is the concentration of iron and dT/dt is the initial slope.
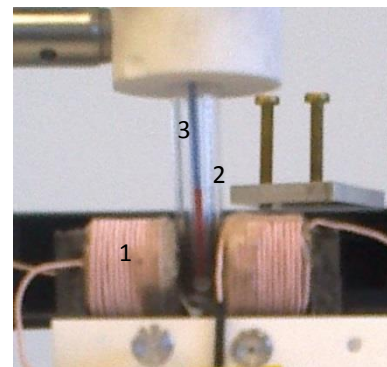
Fig6. Image of the calorimetry set up : 1) magnet, 2) glass flask, 3) temperature probe.

4.2 Magneto optic faraday effect magnetometer

We have measured the hysteresis loops of MNPs that define the energy dissipation using the angle of rotation angle of a polarized beam going through the sample as a function of the applied field, fig 7. This rotation of the light is known as *Faraday effect*.

The Faraday rotation can be related to the magnetization of the sample through the following expression (del Real, 2004):

$$\theta_{rot} = A(\lambda, t) \, M \quad (9)$$

Where A (λ,t) is a constant that will depends on the wavelength (λ) and the sample thickness (t).

Fig 7. Hysteresis loop for γFe₂O₃/SiO₂ using MOFE magnetometer (Gerrero, 1997)

In our set-up, one polarizer is placed in front of the sample in order to define the polarization angle of a 632 nm laser beam that impacts in the sample. After crossing the sample subjected to alternating magnetic field, the polarization direction has been rotated with respect to the initial polarization direction. Then, a Wollaston prism allows splitting the two polarization components in two different beams which reach respective photodetectors. Analyzing both components is possible to extract the angle of rotation and consequently the hysteresis loop of the sample. The magnetic field is applied by an air-refrigerated coil surrounding the sample which is connected to a LCR circuit similar to the one used for calorimetry measurements.

The hardest difficulty to obtain the hysteresis loops from MNP is that the magnetic material is just a small part of the system dispersed in a solvent. Thus, the sample is usually dry to study the powder formed. But these analyses modify the magnetic interactions of the MNP.

The MOFE allows extracting in a quick and precise manner, the hysteresis behavior of the MNP in suspension at different frequencies without changing any condition of the system except the concentration. It is necessary to dilute the ferrofluid to 0,3 mg/ml to preserve the intensity of the transmitted light and obtain accurate measurements.

The main drawback of this technique with respect to other magnetometers is that one cannot quantify the A (λ,t) constant to extract the magnetization values. However, the wide qualitative information provided by MOFE allows monitoring the evolution of coercitive fields from mHz up to hundreds of KHz with a single requirement: high colloidal stability of the MNP dispersion that ensures an adequate magneto-optic response.
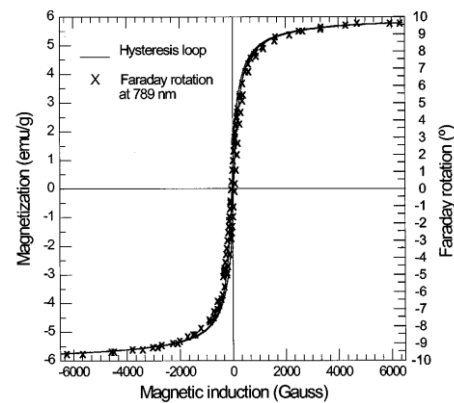
5. EXPERIMENTS

5.1 STRUCTURAL AND COLLOIDAL CHARACTERIZATION

In this project three nanoparticle samples have been synthetized:

1. MNP of 12 nm prepared in water by co-precipitation of Fe (II) and Fe (III) salts.
2. MNP of 17 nm, prepared by thermal decomposition in organic media.
3. MNP of 22 nm, prepared in water by precipitation of a Fe (II) salt.

Fig 8 shows the pictures obtained by TEM of these three samples and the histograms of their size distributions fitted by a lognormal function.
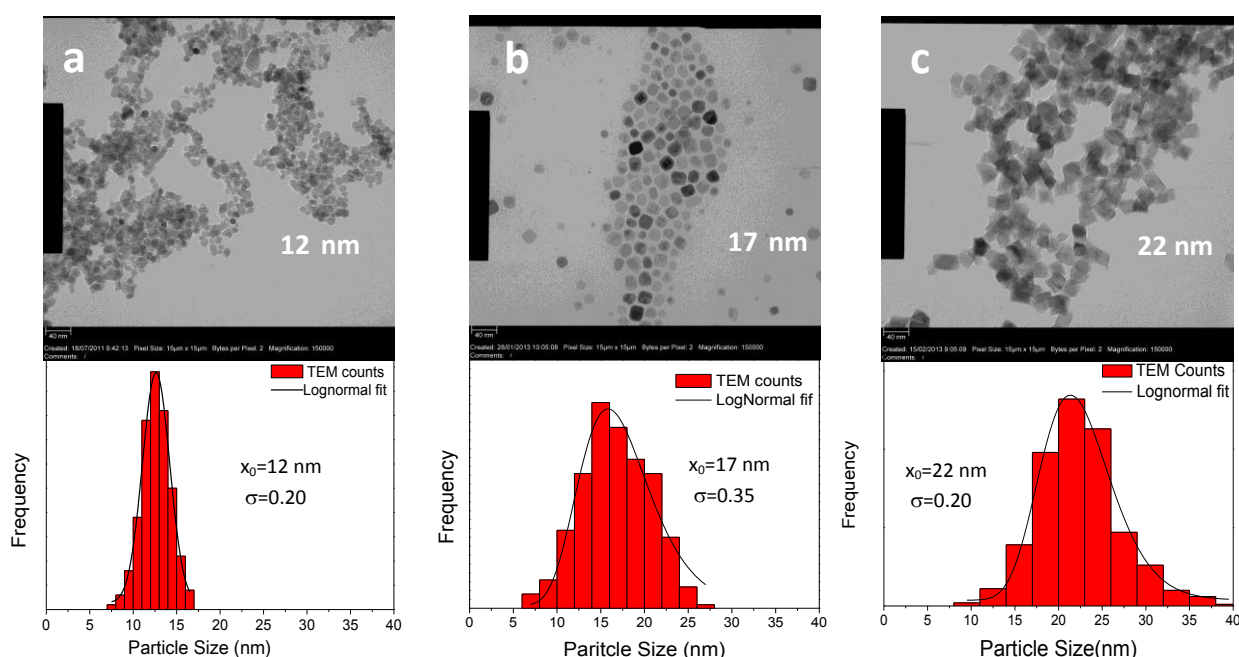

Fig 8. TEM images of the three systems 12 (a), 17(b) and 22 nm (c) and their correspondent size distribution and fittings.

The crystalline structure obtained by an X-ray diffraction, fig 9, for the three sizes shows a similar peak positions. The patterns unveil the presence of two possible magnetic phases, maghemite and magnetite, which could only be distinguished by more advanced techniques (Espinosa, 2012).
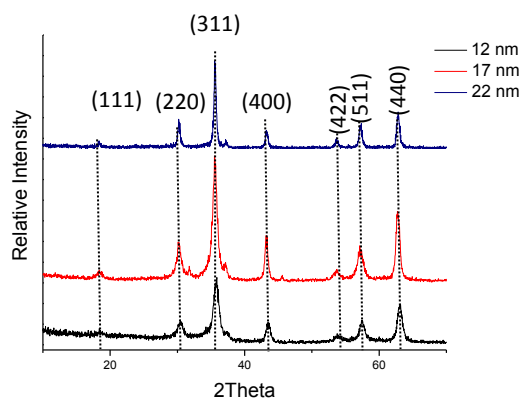

Fig 9. X-ray diffraction for the three collection of MNP

Nevertheless it is also possible to extract information about the crystal size from the width of the peaks. The results obtained from the (311) peaks are contained in Tab 1 where we can

observe that the size of the crystal is quite similar to the size obtained for the nanoparticles observed by TEM, what implies a high crystallinity for the MNP.

Finally, we have performed a thermogravimetric analysis of the samples, fig 10. For 18 nm and 22 nm MNP, it can be observed a weight increase at the beginning of the graph which suggests the presence of a magnetite core that is oxidized during the heating, and increases the sample's weight. At high temperatures the curve falls due to the evaporation of the coating.
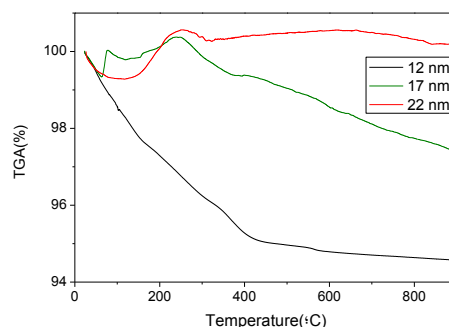

Fig 10. Thermogravimetry analysis (TGA) for the three collections of MNP

The difference between the maximum and minimum of weight is a good approximation to estimate the amount of organic material present in the sample and evaporated during the process as CO_2. Relative losses of weigh are included in Tab 1. Between 5 and 10 % is the percentage expected from a monolayer of DMSA molecules at the nanoparticle surface, decreasing as the particle size increases.

Particle size(nm)	Standard deviation	Crystal size (nm)	Isoelectric point	Hydrodynamic size, D_H (nm)	Polydispersity Index PDI	Organic material
12	0.20	11	1.5	52	0.14	5.5 %
17	0.35	12	1.5	69	0.10	3.5 %
22	0.20	30	1.5	76	0.09	1 %

Tab 1. Colloidal features for the three collection of MNP

5.2 CALORIMETRIC MEASUREMENT

After structural and colloidal characterization, it is possible to begin the calorimetric study. Fig 11 shows the values of SAR obtained at different magnetic field amplitudes and frequencies when the samples are dispersed in media with distinct viscosity, water and agar. For agar preparation, the MNP were dispersed in suspensions with 10% in weight of dry agar. That solution produces a gel that immobilizes the MNP hampering their rotation.

In all three samples we observe a frequency linear dependence of the energy dissipated as expected from theory (eq. 2). But the quadratic growth with the field amplitude is observed just for the 18 nm nanoparticles, the rest have been fitted using different powers.

It is worth to notice how the SAR presents different dependence with the media viscosity for each size. The measurements made on agar differ from the ones made in water in around 20% for 12 nm MNP, 45 % for 18 nm and 60% for 22 nm.
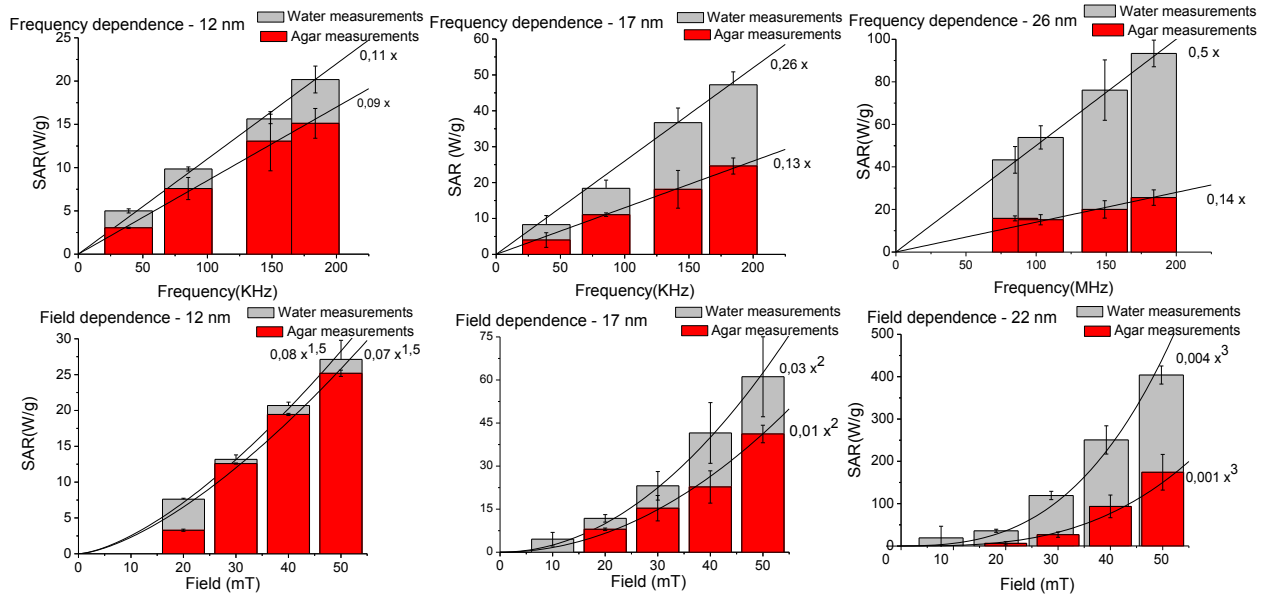

Fig 11. Firs row, SAR measurements at constant field of 25 mT for 12 nm, 17 nm and 22 nm. Second row, SAR measurements at constant frequency of 85 KHZ for the same sizes. They have been included the respective regressions.

Such behavior can be explained in terms of size dependence of Brown and Néel relaxation processes. For the 12 nm MNP, the change in the viscosity of the media does not affect to its heat generation capacity, what suggests that most of the particles presents a Néel relaxation mechanism for which the media viscosity is not relevant (eq. 4). On the contrary, the great discrepancies between both media for 22 nm MNP reflect their preference for Brownian rotation.

These results are in agreement with previous studies carried out at the University of Paris (Fortin, 2007). They calculate Néel and Brownian relaxation times for MNP with different anisotropy constant (maghemite and cobalt ferrite) soaked in dispersant of different viscosity (water and glycerol), fig 12.

We can appreciate in the dot line (maghemite in water) that for MNP of 12 nm, the Néel relaxation is the faster, while for 22 nm the Brownian rotation is the one which
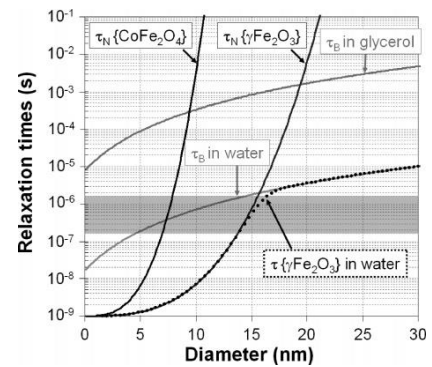

Fig 12. Graphical representation of the τ_N for maghemite (γFe_2O_3) and cobalt ferrite ($CoFe_2O_4$) MNP and τ_B for water and glycerol. The point line will be the reference in the present study. (Fortin, 2007)

leads the process. About the mid-size 18 nm both contributions seems to be relevant to the relaxation process. Because of that, and because the large SAR values observed, we have chosen those MNPs for the next step, the aggregation effects study.

Before to conclude this section, it is necessary to point out that the nanoparticles of 22 nm produce a considerable amount of heat comparing them with the values that appear in the bibliography (Boubeta,2013). However, their dependency with the media viscosity could mean a problem for Hyperthermia applications in biology media where the viscosity is hard to determine because it introduces an uncontrolled factor in the treatment.

5.3   AGREGATION EFFECTS STUDY

In this section, we evaluate the influence of aggregation state of MNP on SAR values. The way chosen to produce the aggregation was to disperse the MNP in a tampon solution with a specific pH at which their surface charge should decrease.

The decreasing of the superficial charge produces a minor repulsion between the nanoparticles and after sometime an increase of the aggregate size. This idea has been previously faced with MNP of smaller size recovered with polymers (Park Y., 2012) where the steric repulsion was remained to minimize the instabilities produced by the pH change. Nevertheless, these experiments take more than a month to observe growths in the aggregate size, what was not assumable for a project of three months.
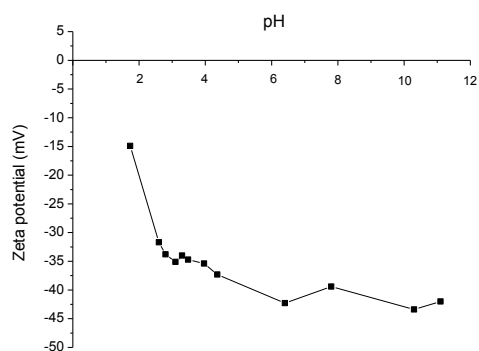
Fig 13. Representation of zeta potential at different pH for MNP of 18 nm.

To carry out a controlled aggregation process it was necessary to take into account how the zeta potential changes with the pH in order to ensure soft instabilities. The evolution of zeta potential with pH is showed in fig 13. Considering this curve, we decided to work with pH's around 4 to grow up the aggregates in a controlled way.

After dispersing the MNP in tampon solutions of potassium hydrogen phthalate and sodium hydroxide at pH 4.4 and 4.2, ultrasounds were applied to the samples in order to break the biggest clusters. Finally, the hydrodynamic sizes obtained for the aggregates were 150 and 570 nm with a polydispersity index of 0.24 and 0.22 respectively.

The calorimetry measurements in water and agar were repeated for the new aggregate sizes and compared with the one dispersed at pH 7 where the D_H was 70 nm (tab 1). In all these measurements the magnetic material concentration of the samples has been maintained constant at 2,5 mg/ml. In fig 14 we observe a progressive decrease of SAR with the aggregate size for both media, but how this drop occurs is something that requires to be discussed.

Looking at the results of MNP dispersed in water, the evolution is clear, the bigger is the aggregate the smaller is the heat dissipated. This fall confirms the *in-vitro* experiments exposed in the introduction where the heat generated decreases inside the cells due to the encapsulation of the MNP in the endosomes.
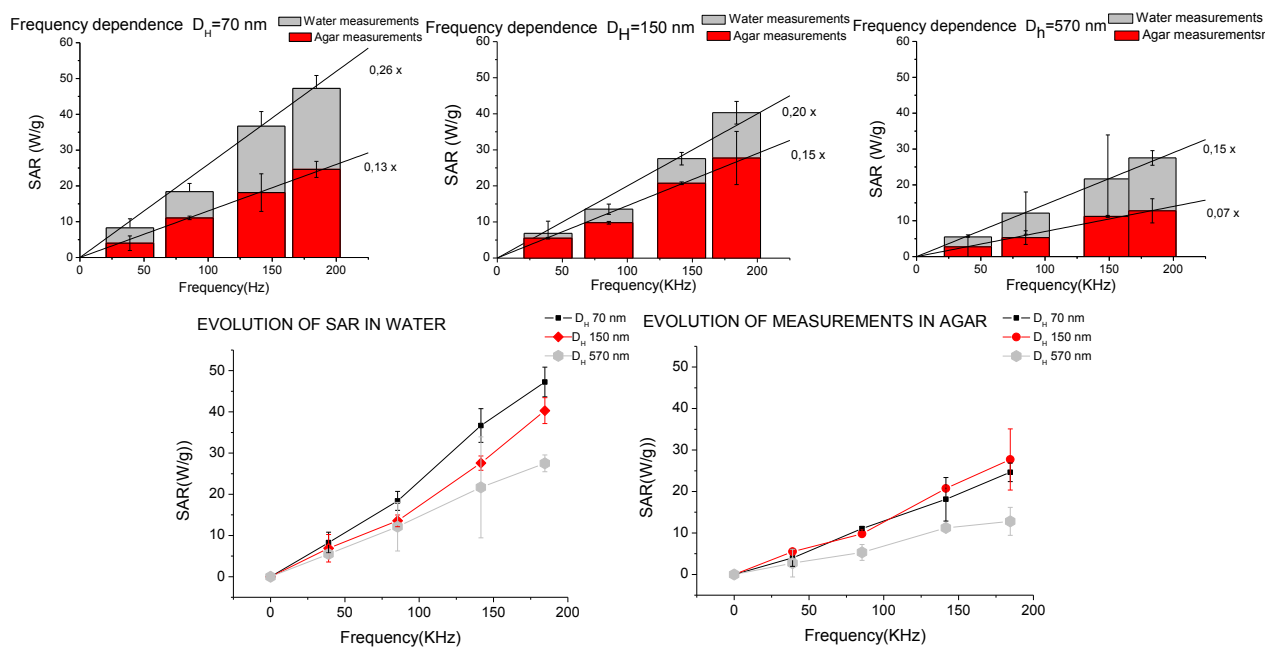

Fig 14. Evolution of SAR measurements at 25 mT with the growth of aggregate size. The upper graphs represent the water and agar measurements in each aggregation state, from left to right 70, 150 and 560 nm. The lower row show the SAR measured at different D_H in both media.

Besides, it is well known that the pH in late endosomes decays until 5.5 (Dikic, 2006). Because of that, we would expect that the aggregation process inside them will follow similar evolution to those reproduced in our experiments.

On the other hand, if we analyze the measurements performed in agar, we observe that surprisingly the SAR does not decrease from 70 to 150 nm. It is necessary to growth up eight times the size of the aggregate to observe a reduction of the SAR value. Therefore, we can conclude that the SAR values variation for 70 and 150 nm must be related with some mechanical process which depends on the media viscosity.

We propose two possible explanations to the observed data. The first considers that the growth of the hydrodynamic size reduces the number of aggregates in the dispersion, i. e., the same amount of material gather in big clusters produces less number of clusters. Therefore, in water, the number of rotating aggregates decreases and, despite each aggregate produces more heat due to its bigger size, the total amount of heat decays.

In agar, where the aggregates are physically blocked, the process is quite different because the magnetic moments of the nanoparticles rotates inside the particles independently until the point where the magnetic interactions are big enough to lead to collective magnetic behavior and reduce in the heat dissipated (D_H =560 nm).

The second explanation is based on the fact that the samples present a different polydispersity index (0.24 for DH=150 and 0.20 for DH=560 nm). Hence, when those MNP with multiple aggregate sizes are dispersed in agar the biggest ones keep blocked and cannot rotate. Only the smallest ones contribute to the heat, producing a reduction in the heat generated.

5.4 OPENING OF THE MAGNETIC CYCLE

To conclude, we complemented the previous measurements with a direct analysis of the aggregation effects over the MNP's hysteresis loops. To perform this study the MOFE magnetometer mentioned in the introduction has been used.

In the fig 15 are presented the results of the hysteresis loops obtained for stable MNP of 18 nm dispersed in water at pH 7 (D_H = 70 nm). A magnetic field of 25 mT at different frequencies (0,3-30 KHz) was applied to perform the cycles. On the right hand the coercitivity fields of the different loops are collected to observe the frequency at which the cycle opens.

We can observe hysteretic behavior at frequencies over 1Hz ; below it, the cycles remains closed. Consequently, the relaxation time at room temperature for this MNP ought to be around 1 second which represents the theoretical limit of superparamagnetism. The area of the different hysteresis loops *could* be related with the heat generated at different frequencies through the (eq. 2) by multiplying the cycle area (A= ΔU) and the frequency of the applied field.
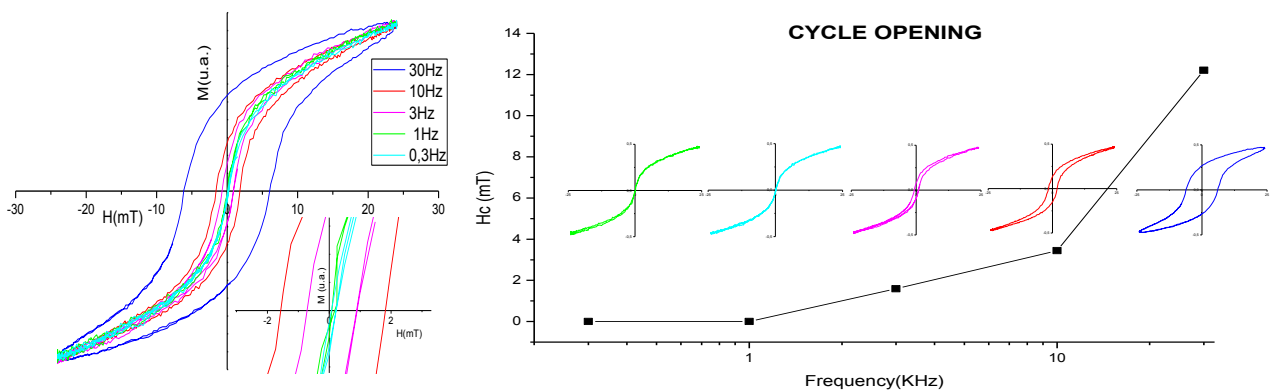

Fig 15. Hysteresis loops at different frequencies for MNP of 18 nm and their coercivity fields

Unfortunately the Faraday magnetometer does not provide a quantitative value of this area. Nevertheless, the comparison of normalized magnetization cycles allows establishing relative changes of area and analyzing the aggregation effects over the heat generated.

As was explained in the section 4.1, the technique requires a certain colloidal stability of the sample. Because of that, only two aggregation states (D_H 70 and 350 nm) could be measured. Both cases were measured at 30 KHz and 25 mT. The results are presented in fig 16.

The bigger aggregate shows a clear diminishing of the magnetization cycle area, which provides an explanation to the data obtained previously. The reduction of the hysteresis loops

area during the aggregation produces a reduction in the heat dissipated during the magnetization process and consequently the SAR values also fall.

In the end, we have been able to obtain by direct and indirect measurements, results that proof the reduction of the heat dissipated by the MNP when are arranged in big aggregates.
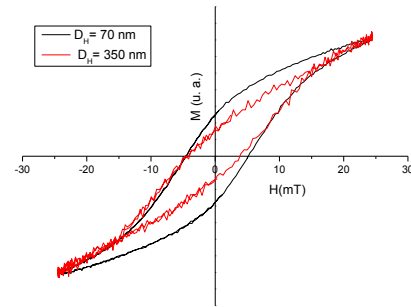

Fig 16. Reduction of the coercivity of MNP of 17 nm due to aggregation at 30 KHz and 25 mT

6. CONCLUSIONS

The present work pretends to systematically analyze the influence of MNP aggregation size on the magnetization properties in order to understand its role on the heat dissipation processes. This roll will be crucial for the biomedical application of the MNP.

After the analysis of the obtained results, we can conclude that:

- The increase of media viscosity produces in all the analyzed cases a reduction in the heating capacity of the nanoparticles dispersed. Furthermore we have observed that the decrease becomes more relevant the bigger the nanoparticles are.

- The calorimetry measurements at different MNP sizes suppose an experimental support to the relaxation mechanisms proposed by Rosensweig (Rosensweig, 2002).

- The aggregation state of MNP systems affects to the heat generated when are submitted to alternate magnetic fields. The reduction in the SAR value due to the aggregation process fits quite well with the previous *in-vitro* experiments reported in the bibliography.

- Finally, the measurement of magnetization cycles carried out with MOFE magnetometer provides a direct measurement of the causes of SAR reduction with the aggregate size. Bigger aggregates present closer hysteresis loops and consequently the heat dissipated decrease.
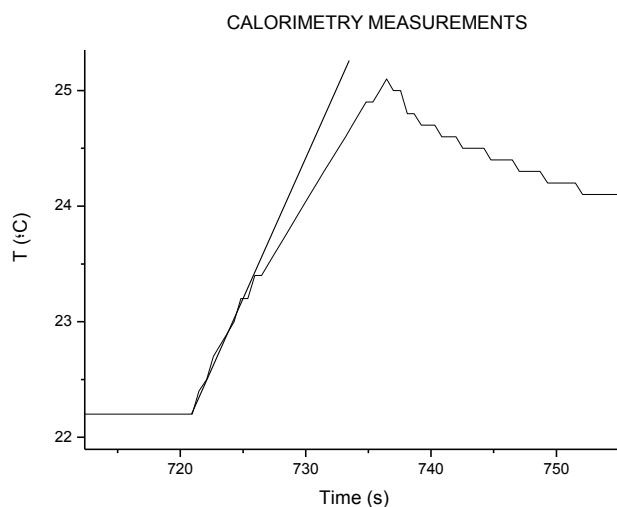
7. APPENDIX AND ACRONYM GLOSSARY

7.1 APPENDIX

CALORIMETRY MEASUREMENTS

Fig 17. Initial slope fitting of the heating curve used in SAR measurements.

7.2 ACRONYM GLOSSARY

D_H	Hydrodynamic size
DMSA	Di Mercato Succinic Acid
ICP-OES	Inductively Coupled Plasma Optical Emission Spectrometry
MNP	Magnetic Nanoparticle
MOFE	Magneto Optic Faraday Effect magnetometer
PDI	Polydisperisty Index
SAR	Specific Absorption Rate
SEM	Scanning Electron Microscopy
TEM	Transmission Electron Microscopy
TGA	Thermogravimetric Analysis
τ_B	Brownian relaxation time
τ_N	Néel relaxation time

8. BIBLIOGRAPHY

A. Durdureanu-Angheluta, L. P. (2008). Silane covered magnetite particles. preparation and characterization. *DJNB,*, 3: 33–40.

Alivisatos, e. a. (1999). A new nonhydrolytic single-precursor approach to surfactant-capped nanocrystals of transition metal oxides. *Journal of American Chemical Socity*, 121,(49), 11595-11596.

Anamaria Durdureanu-Angheluta, M. P. (n.d.). *Materials Science and Technology: Tailored and Functionalized Magnetite Particles for Biomedical and Industrial Applications.*

Brazel C.S., e. a. (1996). Pulsatiles local delivery of thrombolytic and antithombotic agents using poly(N-isopropylacrylamide-co-methacrylic acid) hydrogels. *J. Control Release*, 39:57-64.

Brown, W. (1963). Thermal fluctuations of a single-domain particle. *Jr. Phys. Rev.*, 130:1677.

Chang, e. a. (1993). Synthesis and evaluation of colloidal magnetic iron-oxides for the site-specific radiofrequency-induced hyperthermia of cancer. *J. Magn. Magn. Mater* , 122:374-8.

Chilkoti A., e. a. (2002). Targeted drug delivery by thermaly responsive polymers. *Adv. Drug Deliv. Rev.*, 68:34-45.

delReal R. F., e. a. (2004). Magneto-optical apparatus to measure ac magnetic susceptibility. *Rev. Sci. Instrum.*, 75,N 7, 2351-2355.

Dikic, I. (2006). *Endosomes.* Gerogetown, Texas 78626 ,USA: SpringerScience + Business Media, LLC.

Edwin L. Crow, K. S. (1988). *Lognormal Distributions: Theory and Applications.* CRC, Taylor& Francis.

Espinosa A., e. a. (2012). On the discrimination between magnetite and maghemite by XANES measurements in fluorescence mode. *Meas. Sci. Technol.*, 23, 015602(6pp).

Fortin, e. a. (2007). Size-Sorted Anionic Iron Oxide Nanomagnets as Colloidal Mediators for Magnetic Hyperthermia. *J. Am. Chem. Sox.*, 129:2628-2635.

Frenkel, J. (1855). *The kinetic Theory of Liquids.* New York: Dover Publications.

Gerrero H., e. a. (1997). Faraday rotation in magnetic γ-Fe2O3/SiO2 nanocomposites . *Appl. Phys. Lett.*, 71,(18), 2698-2700.

Getzlaff, M. (2008). *Fundamentals of Magnetism.* Springer.

Gilchrist, e. a. (1957). Selective Inductive Heating of Lymph Nodes. *Annals of Surgery*, vol 146, 4, p. 596-606.

Hergt, e. a. (2008). Effects of size distribution on hysteresis losses of magnetic nanoparicles fo hyperthermia. *J. Phys.: Condens. Matter*, 20:385214 (12pp).

Hunter, R. J. (1993). *Introduction to Modern Colloid Science.* Midsomer Norton: Oxford Science Publications.

I. Martinez-Mera, M. E.-H.-A. (2007). Synthesis of magnetite nanoparticles without surfactant at room temperature. *Mater. Lett.*, 61: 4447-4451.

J.p. Fortin, e. a. (2008). Intracelllular heating of living cells through Néel relaxation of magnetic nanoparticles. *Eur Biophys J*, 37:223-228.

Jordan, A., & al., e. (1999). Endocytosis of destran and silan-coated nanoparticles and the effect of intracillular hyperthermia on human mammary carcinoma cells in vitro. *J. Magn. Magn. Mater.*, 194(1):185-96.

Jordan, e. a. (1993). Inductive heating of ferrimagnetic particles and magnetic fluids: Physical evaluation of thier potential for hyperthermia. *Int. J. Hyperthermia*, 9(1):267-84.

Lee, e. a. (2011). Exchange-coupled magnetic nanoparticles for efficient heat induction. *Nature nanotech.*, 6:418-422.

Mahmoudi M., e. a. (2009). Cytotoxicity and cell cycle effects of bare and poly(vinyl alcohol)-coated iron oxide nanoparticles in mouse fibroblast. *Adv. Eng. Mater.*, 11(12):B243-50.

Maier-Hauff. (2007). Intracranial thermotherapy using magnetic nanoparticles combined with external beam radiotherapy: Results of a feasibility study on patients with glioblastoma multiforme. *J Neurooncol*, 81:53–60.

Maier-Hauff. (2011). Efficacy and safety of intratumoral thermotherapy using magnetic iron-oxide nanoparticles combined with external beam radiotherapy on patients with recurrent glioblastoma multiforme. *J Neurooncol* , 103:317–324.

Massart. (1981). *Preparation of aqueous magnetic liquids in alkaline and acidic media. IEEE Trans Magn., 17: 1247-1248.*

Matijevic, T. S. (1979). Formation of Uniform Spherical Magnetite Particles by Crystallization from Ferrous Hydroxide Gels. *J. Colloid Interface Sci.*, 74, 1 , 227-243.

Mehdaoui, e. a. (2011). Optimal Size of Nanoparticles for Magnetic Hyperthermia: A combined Theoretical and Experimental Study. *Adv. Funct. Mater.*, 21:4573-4581.

Mejías R., e. a. (2011). Dimercaptosuccinic acid-coated magnetite nanoparticles for magnetically guided in vivo delivery of interferon gamma for cancer immunotherapy. *Biomaterials*, 32, 2938-2952.

Mejías, e. a. (2011). *Dimercaptosuccinic acid-coated magnetite nanoparticles for magnetically guided.* Biomaterials 32 2938e2952.

Pachoudhury, e. a. (2011). Synthesis and Growth Mechanism of Iron Oxide Nanowhiskers. *Nano Lett.*, 11, 1141-1146.

Park Y., e. a. (2012). Stability of Superparamagnetic Iron Oxide Nanoparticles at different pH Values:Experimental and theoretical analysis. *Langmuir*, 28,6246-6255.

Park, e. a. (2004). Ultra-large-scale syntheses of momodisperse nanocrystals. *Nature materials*, vol 3, 891-895.

Rosensweig. (2002). Heating magnetic fluid with alrernation magnetic field. *J. Magn. Magn. Mat.*, 252:370-374.

Salas, e. a. (2012). Controlled synthesis of uniform magnetite nanocrystals with high-quality properties for biomedical applications. *J. Mater. Chem.*, vol 22, 21065-21075.

Teran, e. a. (2012). Accurate determination of the specific absorption rate in superparamagnetic nanoparticles under non-adiabatic conditions. *Appl. Phys. Lett.*, 101, 062413.

Villanueva, e. a. (2009). The influence of surface functionalization. *Nanotechnology*, vol 20, 115103 (9pp).